JOURNAL OF SPACECRAFT AND ROCKETS
Vol. 39, No. 6, November–December 2002

# Estimation and Prediction of Orbital Debris Reentry Trajectories

Jason M. Tardy* and Craig A. Kluever†
*University of Missouri–Columbia, Columbia, Missouri 65211*

**Tracking and prediction of orbital debris trajectories have recently received a great deal of attention due to the increasing proliferation of such objects and the hazard they pose to operational spacecraft. Most analyses have focused on in-orbit dynamics, such as the probability of collision with low-orbiting satellites, especially the International Space Station. Less attention has been given to the problem of reentry estimation and impact prediction. During reentry, aerodynamic forces dominate the dynamics, which presents a challenge to the trajectory estimation problem because the relevant characteristics of debris (size, shape, and mass) needed to model the trajectory accurately are largely unknown. A ground-based trajectory estimation method is described that attempts to determine simultaneously the unknown time-varying ballistic coefficients with the state vector using an extended Kalman filter. This filter estimates the unknown ballistic coefficients by using dynamic process noise parameters based on an integral state model. A posteriori information from the filter is processed by a Monte Carlo algorithm to predict the impact location. Simulation results are presented and suggest a high degree of accuracy in both the estimation and prediction stages.**

## Nomenclature

| | | |
|---|---|---|
| $a$ | = | semimajor axis, km |
| $\boldsymbol{a}$ | = | aerodynamic acceleration vector, m/s$^2$ |
| $C_D$ | = | drag coefficient |
| $C_L$ | = | lift coefficient |
| $e$ | = | eccentricity |
| $F$ | = | Jacobian matrix of the governing equations of motion |
| $\boldsymbol{f}$ | = | vector of governing equations of motion |
| $\boldsymbol{g}$ | = | gravitational acceleration vector, m/s$^2$ |
| $H$ | = | Jacobian matrix of measurement model |
| $\boldsymbol{h}$ | = | measurement model |
| $I$ | = | identity matrix |
| $i$ | = | inclination, deg |
| $J_2$ | = | Earth oblateness constant |
| $K$ | = | Kalman gain matrix |
| $m$ | = | mass, kg |
| $P$ | = | error covariance matrix |
| $p$ | = | square root of drag ballistic coefficient, $\sqrt{\beta_D}$ |
| $Q$ | = | spectral density of process noise |
| $\boldsymbol{q}$ | = | Gaussian process noise |
| $\bar{q}$ | = | dynamic pressure, N/m$^2$ |
| $R$ | = | debris radius, m |
| $R_e$ | = | local Earth radius, km |
| $\boldsymbol{r}$ | = | position vector, km |
| $S$ | = | frontal area, m$^2$ |
| $t$ | = | time, s |
| $\boldsymbol{v}$ | = | velocity vector, km/s |
| $v_{\text{rel}}$ | = | Earth-relative velocity, km/s |
| $W$ | = | variance matrix for measurement noise |
| $\boldsymbol{w}$ | = | Gaussian measurement noise |
| $\boldsymbol{x}$ | = | state vector of the reentry object |
| $\hat{\boldsymbol{x}}$ | = | estimated state vector of the reentry object |
| $\bar{\boldsymbol{x}}$ | = | mean of all samples |
| $\boldsymbol{y}$ | = | measurement vector |
| $\beta_D$ | = | drag ballistic coefficient, m$^2$/kg |
| $\beta_L$ | = | lift ballistic coefficient, m$^2$/kg |
| $\delta$ | = | Dirac delta function |
| $\varepsilon$ | = | surface distance error, km |
| $\eta$ | = | ablation constant, m$^2 \cdot$ s/kg |
| $\kappa$ | = | cross correlation |
| $\nu$ | = | true anomaly, deg |
| $\rho$ | = | atmospheric density, kg/m$^3$ |
| $\rho_{\text{debris}}$ | = | debris density, kg/m$^3$ |
| $\sigma$ | = | standard deviation |
| $\Phi$ | = | state transition matrix |
| $\psi$ | = | design constant |
| $\Omega$ | = | right ascension of the ascending node, deg |
| $\omega$ | = | argument of periapsis, deg |

*Subscripts*

| | | |
|---|---|---|
| az | = | azimuth |
| el | = | elevation |
| $i$ | = | measurement index |
| lat | = | latitude |
| lon | = | longitude |
| 0 | = | initial value |

*Superscripts*

| | | |
|---|---|---|
| $+$ | = | updated value |
| $-$ | = | a priori value |

Received 23 May 2001; revision received 24 April 2002; accepted for publication 29 April 2002. 

*Graduate Student, Mechanical and Aerospace Engineering. Student Member AIAA.

†Associate Professor, Mechanical and Aerospace Engineering. Associate Fellow AIAA.

## Introduction

In recent years, the number of nonoperational objects in low Earth orbit has increased dramatically. The problem this presents to ongoing space missions has long been recognized, and much effort has been made to accurately determine, catalogue, and predict the orbital characteristics of these objects to avoid collisions. Most of this effort has been directed at on-orbit operations such as the space shuttle and International Space Station.[1–6] Fewer studies have attempted to estimate and predict the trajectories of debris during atmospheric reentry. This lack of analysis is primarily due to the difficulty in establishing the aerodynamic characteristics of these objects. The growing threat posed by debris provides motivation for more accurate methods of reentry estimation and prediction.

Previous research in reentry trajectory prediction has focused on reentry vehicles. Mehra[7] investigated several nonlinear filters for tracking reentry vehicles. Trujillo[8] used maximum likelihood estimation to determine the lift and drag characteristics of the Space Shuttle Orbiter during reentry. Cardillo et al.[9] used a Kalman filter to estimate uncertain drag profiles for reentering ballistic missiles. Recently, Rao[10] introduced an estimation scheme for predicting orbital debris reentry trajectories.

Currently, U.S. Space Command uses a nonlinear least-squares method to track and predict debris trajectories. This technique has the unfortunate drawback of incorporating force model errors into both the state estimate and error covariance.[11] Inherent in this form of differential correction is an assumed parameterization of the ballistic coefficients. Such a deterministic approach may be sufficient at higher altitudes where density (and, therefore, aerodynamic forces) play a lesser role, but is inadequate for reentry analysis. An alternative approach is to model the dynamics stochastically; this method not only addresses the uncertainty in the ballistic coefficients, but also accounts for measurement errors.

Rao[10] proposed using an integral state to model the ballistic coefficients from within an extended Kalman filter (EKF). This model estimates the coefficients as an integral of stationary white noise and adjoins them to the position and velocity vectors to create an augmented state. In essence, this approach uses random walk in the dynamic model, with the spectral densities of these artificial disturbances as variances of the process noise. Measurements were in the form of azimuth and elevation angles from space-based sensors in high Earth orbit.

This study differs from the preceding one in several ways. Measurements are made from ground-based stations and include range as an estimated parameter. In addition, a dynamic integral state is implemented that tunes itself based on past filter performance. This self-tuning approach has the effect of significantly reducing estimation errors and providing a great deal of stability to the filter. Another important distinction is the use of more advanced atmospheric models in the trajectory simulation and state estimation. Finally, several practical considerations requisite to using ground stations are addressed, including number of tracking stations and their locations, frequency of data, and gaps in measurements.

Although useful in itself, debris trajectory estimation is, in practice, a means to an end, namely, to predict the location of terminal impact. In our analysis, impact prediction is achieved through a Monte Carlo simulation. The basic premise behind this method is simple: Given a number of stochastic parameters and their statistical distributions, repetitive simulations will yield a statistically accurate picture of the process under examination. In this case, given the final covariance of the augmented state, a deterministic model is used to propagate the trajectory to the ground. As the total number of cases becomes large, the impact footprint should converge to a statistically accurate aggregate. Several simulations are presented and compared to demonstrate the effectiveness of this method.

## Optimal Estimation Model

### Estimation

Following Rao,[10] optimal estimation is accomplished through the use of a forward-pass EKF followed by a backward-pass Rauch–Tung–Streibel (RTS) smoother. The EKF estimates nonlinear systems of the form

$$\dot{\boldsymbol{x}} = \boldsymbol{f}(\boldsymbol{x}, t) + \boldsymbol{q}(t) \tag{1}$$

where $\boldsymbol{q}(t)$ is Gaussian process noise with zero mean and variance defined by

$$E\lfloor \boldsymbol{q}(t)\boldsymbol{q}(t)^T \rfloor = Q(t)\delta(t-\tau) \tag{2}$$

where $Q(t)$is the spectral density of $\boldsymbol{q}(t)$. Similarly, discrete measurements are modeled as

$$\boldsymbol{y}_i = \boldsymbol{h}(\boldsymbol{x}_i) + \boldsymbol{w}_i \tag{3}$$

where $\boldsymbol{w}_i$ is Gaussian, zero-mean measurement noise with spectral density $W_i$. The elements of diagonal matrix $W_i$ are the variances of the respective sensors.

The EKF, like its linear counterpart, uses a predictor–corrector scheme. The estimated state vector is

$$\hat{\boldsymbol{x}} = E[\boldsymbol{x}] \tag{4}$$

and the associated error covariance matrix is

$$P = E\lfloor (\boldsymbol{x}-\hat{\boldsymbol{x}})(\boldsymbol{x}-\hat{\boldsymbol{x}})^T \rfloor \tag{5}$$

Given a priori estimates of the state vector and covariance matrix, the Kalman gain is computed as

$$K_i = P_i^- \left(H_i^-\right)^T \left[H_i^- P_i^- \left(H_i^-\right)^T + W_i\right]^{-1} \tag{6}$$

where $H_i$ is the Jacobian matrix of the measurement model $\boldsymbol{h}$ with respect to the states. The optimal update to the estimated state vector is

$$\hat{\boldsymbol{x}}_i^+ = \hat{\boldsymbol{x}}_i^- + K_i \left\lfloor \boldsymbol{y}_i - \boldsymbol{h}\left(\hat{\boldsymbol{x}}_i^-\right) \right\rfloor \tag{7}$$

The error covariance is updated using

$$P_i^+ = \left\lfloor I - K_i H_i^- \right\rfloor P_i^- \tag{8}$$

In the prediction stage of the EKF, the state vector can often be estimated by computing the state transition matrix (STM) from the linearized system matrix. This method suffers from errors due to linearization; however, a more accurate method is to integrate the nonlinear equations of motion numerically,

$$\dot{\hat{\boldsymbol{x}}} = \boldsymbol{f}(\hat{\boldsymbol{x}}, t) \tag{9}$$

The error covariance can be updated in two ways. The first method makes use of the STM, which also suffers from linearization errors, although in many cases the errors are much smaller than those associated with the states. The second method, which is utilized in this analysis, involves numerical integration of the Lyapunov equation[12]:

$$\dot{P} = FP + PF^T + Q \tag{10}$$

The system matrix $F$ is the Jacobian matrix of the governing dynamic equations with respect to the states, evaluated at the estimated state.

### Backward Smoother

The RTS algorithm[13] is a discrete, recursive, fixed-interval backward-sweep smoother. In the following convention, $\Gamma(i|j)$ is read as $\Gamma$ evaluated at point $i$ based on $j$ measurements. The state smoothing equation is

$$\hat{\boldsymbol{x}}(k|N) = \hat{\boldsymbol{x}}(k|k) + A(k)[\hat{\boldsymbol{x}}(k+1|N) - \hat{\boldsymbol{x}}(k+1|k)] \tag{11}$$

where $A(k)$ is the smoothing gain matrix at point $k$ and is computed as

$$A(k) = P(k|k)\Phi^T(k+1|k)P^{-1}(k+1|k)$$
$$k = N-1, N-2, \ldots, 0 \tag{12}$$

The smoothed error covariance is independently calculated as

$$P(k|N) = P(k|k) + A(k)[P(k+1|N) - P(k+1|k)]A^T(k) \tag{13}$$

### Estimator Dynamic Model

As described earlier, the estimation scheme propagates the estimated state by numerically integrating the governing nonlinear equations in the form of Eq. (9). The estimator uses the following dynamic model to predict the motion of a reentry object under the influence of gravitational and aerodynamic forces:

$$\dot{\boldsymbol{r}} = \boldsymbol{v} \tag{14}$$

$$\dot{\boldsymbol{v}} = \boldsymbol{g} + \boldsymbol{a} \tag{15}$$

The gravitational acceleration $\boldsymbol{g}$ consists of two-body gravity and Earth oblateness effects due to $J_2$. Aerodynamic acceleration $\boldsymbol{a}$ comprises lift and drag acceleration components:

$$a_L = \frac{\rho v_{\text{rel}}^2 S C_L}{2m} = \frac{1}{2}\rho v_{\text{rel}}^2 \beta_L \tag{16}$$

$$a_D = \frac{\rho v_{\text{rel}}^2 S C_D}{2m} = \frac{1}{2}\rho v_{\text{rel}}^2 \beta_D = \frac{1}{2}\rho v_{\text{rel}}^2 p^2 \tag{17}$$

Velocity of the object with respect to the rotating Earth atmosphere is $v_{\text{rel}}$. It is assumed that all aerodynamic forces remain in the plane of motion and, therefore, the reentry object's motion is entirely in the vertical plane. In Eq. (17), $p^2$ is substituted for the drag ballistic coefficient $\beta_D$ to ensure the physical constraint of nonnegative drag. Equations (16) and (17) encompass all of the unknown parameters in the aerodynamic acceleration calculations such as lift and drag coefficients, frontal area $S$, and mass $m$. The estimator uses the 1976 Standard Atmosphere for altitudes ranging from 0–127.77 km and the Soviet Cosmos model for altitudes from 127.77–600 km. At an altitude of 127.77 km, the densities of the two models coincide; thus, choosing this altitude to change models ensures piecewise continuity. Density is assumed to be zero above 600 km. Altitude is measured relative to an oblate ellipsoid Earth model with an equatorial radius of 6378.145 km and a polar radius of 6356.752 km.

#### Dynamic Integral State

A new approach is used to estimate the ballistic coefficients. This method, which is termed the dynamic integral state, derives its heritage from the standard integral state and the method of Cardillo et al.[9] The integral state model described by Rao[10] models the ballistic coefficients $p$ and $\beta_L$ as integrals of stationary white noise:

$$\begin{bmatrix} \dot{p} \\ \dot{\beta}_L \end{bmatrix} = \begin{bmatrix} q_D \\ q_L \end{bmatrix} = \boldsymbol{q} \tag{18}$$

These two dynamic equations are appended to the sixth-order state system [Eqs. (14) and (15)] to create an augmented eighth-order system.

Cardillo et al.[9] developed an EKF to track the trajectories of ballistic missiles with uncertain drag. Their approach was to include dynamic components in the process noise covariance matrix. These terms are included in the diagonals of the velocity components of the process noise matrix and are proportional to the square of the estimated velocity error averaged over $n$ previous iterations. In this model from Ref. 9, a constant value is used for the uncertain drag coefficient. Our approach incorporates the basic form of the integral state, Eq. (18), but includes the dynamic velocity noise terms and extends the modification to the ballistic coefficients. Consequently, the process noise covariance matrix is $Q = \text{diag}[0\ 0\ 0\ \ \psi_1 \bar{v}^2_{x_{\text{rel}}}\ \ \psi_1 \bar{v}^2_{y_{\text{rel}}}\ \ \psi_1 \bar{v}^2_{z_{\text{rel}}}\ \ \psi_D \bar{p}^2\ \ \psi_L \bar{\beta}^2_L]$, where $\psi_1$, $\psi_D$, and $\psi_L$ are constant positive design parameters. The velocity component variances consist of the constant $\psi_1$ multiplied by the mean-square residuals of the updated relative velocity components ($\bar{v}^2$ terms), whereas the variances associated with the ballistic coefficients consist of the constants $\psi_D$ and $\psi_L$ multiplied by the mean-square residuals of the updated ballistic coefficients. All residual computations are with respect to the a priori estimate over a predetermined interval and an interval of 50 previous iterations (including the current one) is used for all cases in this study. Before the 50th iteration, residuals are computed from the available data.

In essence, constructing the process noise covariance matrix to depend on the estimated error in velocity allows the filter to evaluate its own performance and tune itself accordingly. When the updates to the velocities are small, the variances of matrix $Q$ diminish to reflect the improved performance and vice versa. Extending dynamic noise to the ballistic coefficients has the effect of damping oscillations about their means. Care must be taken, however, to ensure that the proportionality constants $\psi_1$, $\psi_D$, and $\psi_L$ are large enough to add sufficient noise to the error covariance matrix [see Eq. (10)]; otherwise, the filter will place too much weight on the dynamic model and converge to incorrect values of the ballistic coefficients. This approach has the added benefit of greatly improving filter stability because large errors in the state cause the filter to rely more heavily on the measurements.

Before the development of this model, simulations involving two ballistic coefficients on the same order of magnitude, that is, lifting-type bodies, almost invariably caused the filter to diverge. In contrast, using the dynamic integral state results in remarkably stable and accurate results. Note, however, that the determination of the noise parameters $\psi_D$ and $\psi_L$ is dependent on the mean-square error with respect to the estimated state; thus, measurement errors in the position will propagate to the velocity estimate and introduce errors in the dynamic model. These errors are small, however, and can be ignored.

## Optimal Estimation Results

A number of simulated trajectories were examined, spanning a wide range of initial conditions, ballistic coefficients, and station configurations. A truth, or reference, reentry trajectory is generated by numerically integrating the sixth-order deterministic dynamical model [Eqs. (14) and (15)] with a standard fixed-step, fourth-order Runge–Kutta method. The JGM-3 gravity model with the full $70 \times 70$ field of spherical harmonics is included for accuracy. Density is computed from the 1976 Standard Atmosphere for altitudes below 127.77 km and the Soviet Cosmos model for altitudes between 127.77 and 600 km. Uncertainties in atmospheric density are modeled by including normally distributed random fluctuations in the reentry simulation, where $\pm 3\sigma$ corresponds to $\pm 20\%$ variation in the ideal density model. Therefore, the reentry simulation and the estimation scheme utilize different density models. (The estimation scheme uses the joint 1976 Standard Atmosphere/Cosmos model without uncertainties.)

Ballistic coefficients for the orbital debris vary during reentry due to ablation. Lift and drag ballistic coefficients are

$$\beta_L(t) = \frac{S(t)C_L}{m(t)}, \qquad \beta_D(t) = \frac{S(t)C_D}{m(t)} \tag{19}$$

We assume that the debris is a homogeneous sphere and that it ablates during reentry. Therefore, the ballistic coefficients change due to decreases in debris mass and frontal area. Because frontal area is $S = 4\pi R^2$ and spherical debris mass is $m = 4\pi R^3 \rho_{\text{debris}}/3$, the ballistic coefficients have an inverse relation with debris radius $R$. Radius of the sphere is assumed to decrease due to symmetric ablation at a rate proportional to $S$ and dynamic pressure:

$$\dot{R} = -\eta(S/S_0)\bar{q} \tag{20}$$

where $\eta = 10^{-13}$ m$^2 \cdot$s/kg is the assumed ablation constant. Dynamic pressure is

$$\bar{q} = \tfrac{1}{2}\rho v^2_{\text{rel}} \tag{21}$$

Debris radius is updated during the reentry simulation by using a simple Euler integration method and Eq. (20):

$$R(t + \Delta t) = R(t) + \dot{R}\Delta t \tag{22}$$

where $\Delta t$ is the integration time step. New ballistic coefficients are computed from the updated debris radius and Eq. (19). We use $R_0 = 1$ m for all simulations.

Ground station tracking data consist of range and azimuth and elevation angle measurements taken at fixed intervals. The measurement noise matrix $W$ is a $3 \times 3$ square matrix, $W = \text{diag}[\sigma_{\text{range}}\ \ \sigma_{az}\ \ \sigma_{el}]$. The standard deviations of the respective sensors are $\sigma_{\text{range}} = 10$ m, $\sigma_{\text{az}} = 2 \times 10^{-4}$ rad, and $\sigma_{\text{el}} = 2 \times 10^{-4}$ rad, which are typical of U.S. Space Command sensors.[14] Measurements are simulated by corrupting the reference trajectory (expressed in a topocentric-horizon frame) with noise produced by a Gaussian random number generator. For the case of multiple station data, a composite measurement scheme must be constructed. Assuming all stations have the same level of sensor noise, each station's data are corrupted individually. Measurements are then transformed to geocentric Cartesian coordinates, and the state vector is averaged. This mean trajectory is then converted back to measurement data (range, azimuth, and elevation) at an arbitrary station location and the filter estimates the state from these composite measurements.

#### Filter Tuning

Accurate filter results require proper tuning, or modeling, of process noise. For tuning purposes, ballistic coefficient configurations were first analyzed using a "glass Earth" model for measurements. The glass Earth is a useful abstraction for validating the filter and analyzing the effects of various parameters by ignoring the physical constraint that measurements can only be taken at positive elevation

**Table 1 Ballistic coefficient configurations for filter tuning trials**

| Trial | Initial $\beta_D$, m$^2$/kg | Initial $\beta_L$, m$^2$/kg | $\psi_D$ | $\psi_L$ |
|---|---|---|---|---|
| 1 | $5 \times 10^{-4}$ | $5 \times 10^{-5}$ | $10^{-7}$ | $10^{-11}$ |
| 2 | $5 \times 10^{-3}$ | $5 \times 10^{-4}$ | $10^{-7}$ | $10^{-11}$ |
| 3 | $5 \times 10^{-2}$ | $-5 \times 10^{-5}$ | $10^{-6}$ | $10^{-12}$ |
| 4 | $5 \times 10^{-2}$ | 0 | $10^{-6}$ | $10^{-12}$ |
| 5 | 0.5 | 0.5 | $10^{-6}$ | $10^{-7}$ |

**Table 2 Filter tuning trial statistics**

| Trial | Radial error rms, m | Velocity error rms, m/s | $\beta_D$ Error rms, % | $\beta_L$ Error rms, % |
|---|---|---|---|---|
| 1 | 29.71 | 1.14 | 5.27 | 9.25 |
| 2 | 28.78 | 0.47 | 1.76 | 5.70 |
| 3 | 36.49 | 1.94 | 3.02 | 54.90 |
| 4 | 34.72 | 1.14 | 3.02 | N/A[a] |
| 5 | 243.64 | 11.36 | 0.70 | 0.80 |

[a]Relative lift error cannot be computed for the zero-lift case.

angles. This abstraction allows continuous tracking from a single location, which prevents station location, data gaps, and simultaneous measurements from obscuring the relationship between trajectory variables and filter performance. In this preliminary filter-tuning stage, measurements were taken from a location of 0° latitude and 0° longitude.

The ballistic noise constants $\psi_D$ and $\psi_L$ are tuned by investigating reentry trajectories with a wide range of ballistic coefficients. Combinations of initial $\beta_D$ ranging from $5 \times 10^{-4}$ to 0.5 m$^2$/kg and initial $\beta_L$ from $5 \times 10^{-5}$ to 0.5 m$^2$/kg were considered. For the tuning analysis, the initial orbit elements are $a = 6490$ km, $e = 0.01$, $i = 45$ deg, $\Omega = 0$ deg, and $\omega = 45$ deg, which results in a Keplerian orbit with an apogee altitude of 177 km and a perigee altitude of 47 km. The initial true anomaly is set at 270 deg, and, therefore, the initial altitude is 117 km. Atmospheric density uncertainties were not included in the filter tuning trials. Table 1 presents the variety of initial lift and drag configurations along with the tuned noise parameters. The noise constants $\psi_D$ and $\psi_L$ were adjusted until the errors in position, velocity, and ballistic coefficients were observed to be small in an rms sense. Tuning was performed in a simplex-type manner, iterating over noise parameter combinations in discrete factors of 10. Although no formulistic merit function was used to evaluate the results, ballistic coefficient accuracy was given priority over that of the state because the accuracy of the coefficients is the primary determinant of accuracy in the prediction stage.

Table 2 presents statistics for each tuning trial. The relative magnitude of the ballistic coefficients does not significantly alter the estimation of the trajectory, but it does affect relative errors in the estimation of the coefficients themselves. If the lift is much lower ($\beta_L < 0.01\beta_D$) than the drag, for example, trial 3, the error in the lift coefficient becomes large due to the coupling between the aerodynamic forces. In this scenario, the filter has difficulty determining whether deviations from the measured trajectory are due to drag or to lift. Consequently, a small perturbation in $\beta_D$ will be compensated by a large change in $\beta_L$. This discrepancy is not visible in the estimation of the states, however, because acceleration due to lift is relatively small.

The optimal estimate of the time-varying ballistic coefficients is computed by averaging the smoothed estimate within a predetermined range of altitudes. Averaging the estimates reduces errors due to oscillations about the mean. Extensive analysis over a wide range of scenarios has established that coefficient estimates are most accurate within a certain atmospheric regime. The reason for this trend is twofold. The primary reason is that at extreme altitudes, estimation suffers from the magnitude of the density. At high altitudes, the atmosphere is sparse; as a result aerodynamic forces are small and, therefore, difficult to distinguish from measurement noise. At low altitudes, the dense atmosphere degrades estimation because small errors in estimation have large effects on the filter dynamic model. The second reason is a consequence of all filter-smoother schemes: estimation errors are smallest in the middle of a batch of data because they are framed by the most information.

**Estimation Results**

After tuning the filter for a given ballistic coefficient configuration, realistic entry cases can be considered. This study uses the 14 existing U.S. Space Command dedicated and collateral debris tracking stations to analyze a hypothetical reentry trajectory. For this analysis, the initial conditions were $a = 6546.010$ km, $e = 0.01$, $i = 45$ deg, $\Omega = 230$ deg, $\omega = 40$ deg, and $\nu = 1$ deg. Apogee and perigee altitudes of the initial Keplerian orbit are 233.3 and 102.4 km, respectively. The true initial ballistic coefficients are taken from tuning trial 2[$\beta_D = 5 \times 10^{-3}$ m$^2$/kg and $\beta_L = 5 \times 10^{-4}$ m$^2$/kg]. Station coverage for this simulation is presented in Fig. 1, which shows several measurement gaps. Test cases were run with station measurement frequencies of 0.2, 0.5, 1, and 2 Hz. These frequencies are somewhat less than the 20-Hz measurement capability of existing ground tracking stations.[15] Figure 2 presents the smoothed altitude estimate for the range of measurement frequencies along with the reference (truth) altitude profile. Note that the object makes several skips in and out of the upper atmosphere and finally remains in the atmosphere for reentry after about 160 min. Figures 3 and 4 present the $1\sigma$ confidence levels in radial and velocity estimation for cases with different measurement frequencies. As expected, the errors diminish with higher measurement frequency. Figures 3 and 4 show the clear improvement in estimation accuracy as data accumulate and as the object comes in view of a ground station (note the station coverage times displayed in Fig. 1). The errors also diminish as the debris reenters (and remains within) the atmosphere and the ballistic coefficient estimates improve.

A clearer view of the progress of the estimation process can be obtained by examining the effect of altitude on estimated parameters. Figures 5 and 6 show the smoothed estimates of the time-varying lift

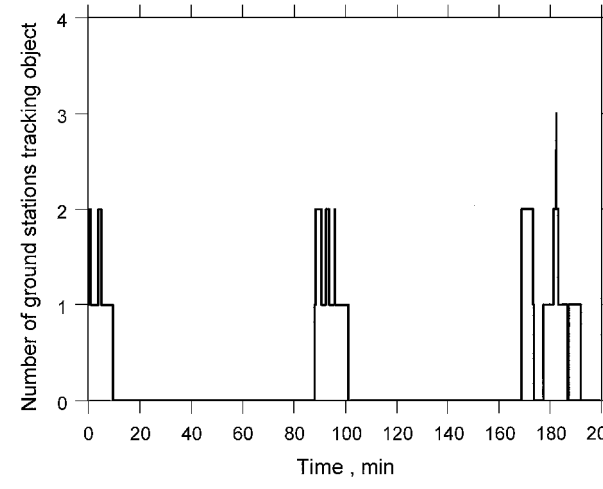


**Fig. 1 Ground station coverage during reentry.**

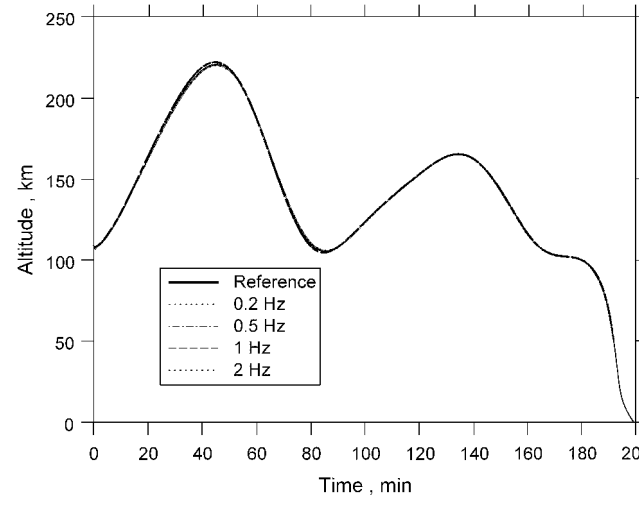


**Fig. 2 Altitude estimation for reentry trajectory.**

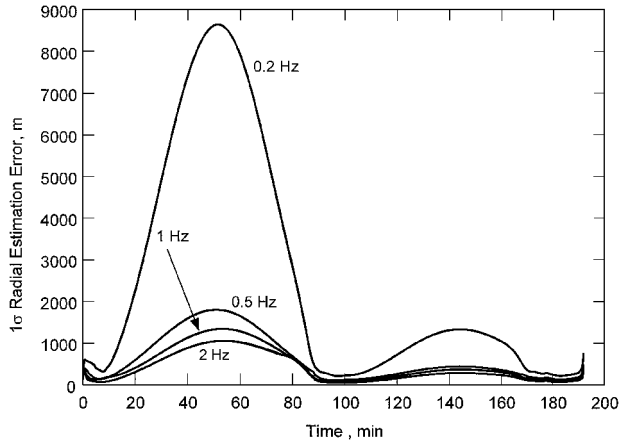


**Fig. 3 Standard deviation of radial estimation error during reentry.**

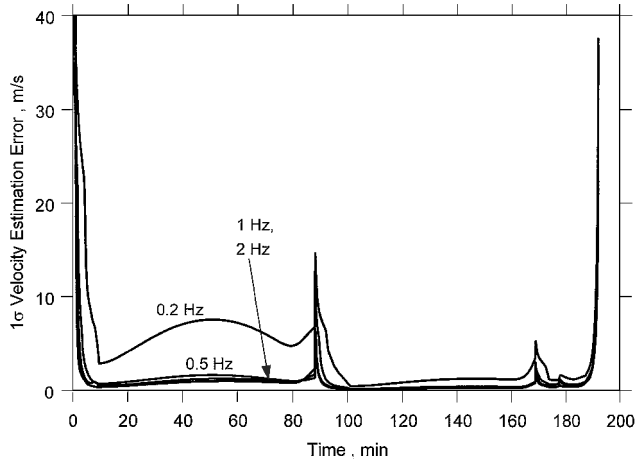


**Fig. 4 Standard deviation of velocity estimation error during reentry.**

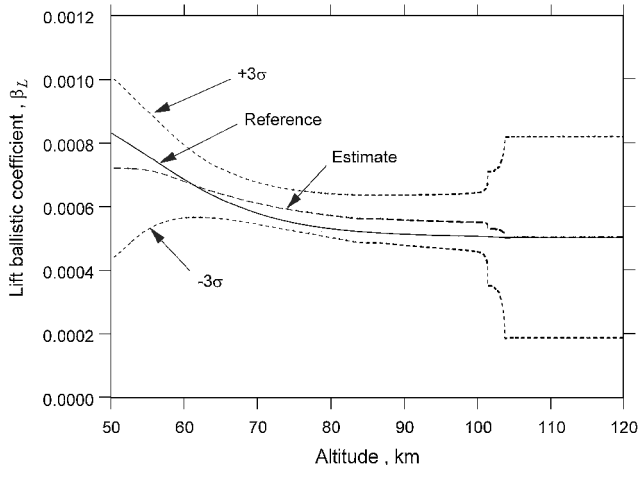


**Fig. 5 Lift ballistic coefficient $\beta_L$ vs altitude (measurement frequency = 0.5 Hz).**

and drag ballistic coefficients and their associated $3\sigma$ error bounds (from the smoothed error covariance) vs altitude during reentry for the 0.5-Hz case. Because altitude is not unimodal (Fig. 2), only the last 37 min of the reentry trajectory is shown. As seen during the early stage of the reentry, the coefficients remain constant when no tracking is available. Figures 5 and 6 demonstrate the estimation filter's ability to produce good estimates of the time-varying ballistic coefficients with the lowest measurement frequency (0.5 Hz).

### Measurement Frequency

Measurement frequency is a crucial factor in filter performance. If measurement frequency is too low, the filter will diverge. Not surprisingly, higher frequencies result in better estimates. Table 3 shows the estimation errors from several reentry trials with a range of measurement frequencies. The velocity error values do not include the first 100 estimates because these are transient and skew the numbers. It is clear from these statistics that measurement frequency has a significant impact on estimation accuracy. In general, the higher the frequency, the better the results, although this improvement seems to be somewhat asymptotical.

**Table 3 Estimation statistics for measurement frequency trials**

| Measurement frequency, Hz | $\psi_D$ | $\psi_L$ | Radial error rms, m | Velocity error rms, m/s | $\beta_D$ Error rms, % | $\beta_L$ Error rms, % |
|---|---|---|---|---|---|---|
| 0.2 | $10^{-8}$ | $10^{-11}$ | 233.43 | 4.85 | 4.45 | 7.81 |
| 0.5 | $10^{-8}$ | $10^{-11}$ | 103.96 | 1.84 | 3.68 | 8.47 |
| 1 | $10^{-7}$ | $10^{-11}$ | 75.81 | 1.88 | 3.43 | 8.63 |
| 2 | $10^{-7}$ | $10^{-10}$ | 63.46 | 2.93 | 2.23 | 6.37 |

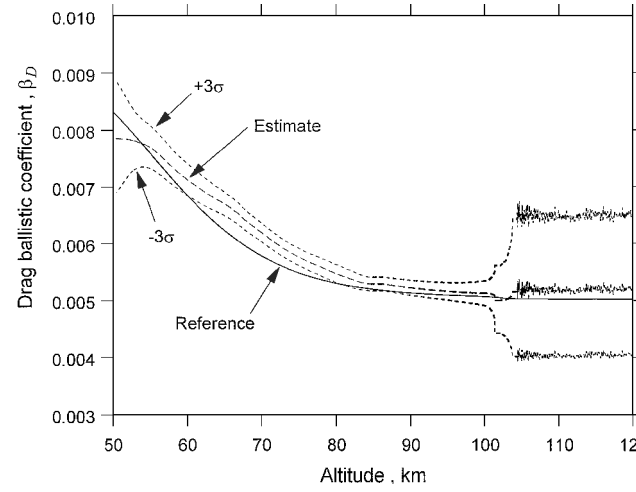


**Fig. 6 Drag ballistic coefficient $\beta_D$ vs altitude (measurement frequency = 0.5 Hz).**

By comparison, the estimation scheme of Rao[10] used measurement frequencies on the order of 0.1 Hz over an altitude range of 65–95 km. (Our estimator is utilized in the 50–116-km altitude range.) Rao presented radial errors of about 2000-m rms and velocity errors of about 20-m/s rms. Ballistic coefficient errors are not numerically specified in Ref. 10, but one figure in Ref. 10 shows an average lift ballistic coefficient estimate of about $3 \times 10^{-4}$ m$^2$/kg for a nonlifting case with $\beta_D = 3.18 \times 10^{-4}$ m$^2$/kg. Rao's work assumes piecewise constant ballistic coefficients (two segments, before and after debris breakup), and his estimation trials involve space-based sensor configurations where at least one sensor is always providing measurements. Our estimation results from the tuning trials (with fictitious continuous ground coverage and 1-Hz measurement frequency) yield radial errors of about 100 m and velocity errors of about 10 m/s. Clearly, higher measurement frequency results in smaller estimation errors.

### Additional Estimation Issues

Several issues merit additional discussion. Satisfactory filter performance is dependent on the availability and location of station coverage along the reentry trajectory. More important, there is a critical zone of estimation for every case, usually between altitudes of 50 and 100 km. Without sufficient tracking during this regime, the filter will quickly diverge. The station configuration used in this study is insufficient for most cases; the filter diverges for simulations without sufficient tracking at lower altitudes. Increasing the number of tracking stations (especially in the southern hemisphere) will alleviate this problem. However, the best solution is to use a network of space-based sensors such as those used by Rao.[10]

As mentioned earlier, the dynamic integral state reduces the accuracy of the error bounds. This reduction can cause erroneous footprints if not taken into consideration when tuning the filter. In addition, the smoother may have problems at lower altitudes if the

noise coefficients are too large. Ill-formed covariance matrices can also degrade filter performance. Using more advanced estimation schemes such as a square-root information filter and an alternative smoother can alleviate this problem.

## Monte Carlo Impact Prediction

Monte Carlo methods are a common way to analyze nondeterministic problems. These methods use a large number of iterations to generate a statistical representation of the outcome of a stochastic process, given the distribution of the random parameters. In this case, reentry trajectories are propagated from the terminal observed altitude (i.e., the altitude at which measurements cease completely) to impact, given the final error covariance from the filter. Statistical conclusions can then be drawn from the resulting footprint. Each iteration corresponds to a sample vector of normally distributed initial conditions, which are input into a dynamic propagator. This propagator includes two-body and $J_2$ gravity terms, as well as lift and drag. The trajectories are propagated to zero altitude and converted to geocentric latitude and longitude.

The covariance of the footprint can be calculated using the law of large numbers. In the context of this analysis, this axiom asserts that as the number of samples becomes large, the integral in the expectation operator can be replaced by a summation:

$$E[F(\boldsymbol{x})] = \int (\boldsymbol{x}_i - \bar{\boldsymbol{x}})(\boldsymbol{x}_i - \bar{\boldsymbol{x}})^T \, \mathrm{d}\boldsymbol{x} \cong \frac{1}{N} \sum_{i=1}^{N} (\boldsymbol{x}_i - \bar{\boldsymbol{x}})(\boldsymbol{x}_i - \bar{\boldsymbol{x}})^T \tag{23}$$

The covariance matrix at impact is

$$P_{\text{impact}} = \frac{1}{N-1} \sum_{i=1}^{N} (\boldsymbol{x}_i - \bar{\boldsymbol{x}})(\boldsymbol{x}_i - \bar{\boldsymbol{x}})^T \tag{24}$$

where the overbar represents the mean of all of the samples. The resulting $2 \times 2$ covariance matrix is

$$P_{\text{impact}} = \begin{bmatrix} \sigma_{\text{lon}}^2 & \kappa \sigma_{\text{lon}} \sigma_{\text{lat}} \\ \kappa \sigma_{\text{lat}} \sigma_{\text{lon}} & \sigma_{\text{lat}}^2 \end{bmatrix} \tag{25}$$

where $\kappa$ is a measure of cross correlation. The $3\sigma$ confidence levels for longitude and latitude can be determined from the diagonals of this covariance matrix.

The true state and the best guess from the filter are also propagated to impact. The full dynamic gravity model is used to integrate these trajectories. Although within the atmosphere, the inclusion of higher-order harmonics affects the outcome by no more than a few kilometers, depending on the simulation. The surface distance error of the best estimate (i.e., the distance from the estimated to the actual point of impact along the surface of the Earth) is

$$\varepsilon^* = R_e \cos^{-1}\left( \frac{\boldsymbol{r}_{\text{true}}^T \boldsymbol{r}^*}{\|\boldsymbol{r}_{\text{true}}\| \, \|\boldsymbol{r}^*\|} \right) \tag{26}$$

In Eq. (26), $\boldsymbol{r}_{\text{true}}$ and $\boldsymbol{r}^*$ are the position vectors of the actual and estimated locations of impact, respectively, and $R_e$ is the local radius of the Earth, averaged between the magnitudes of the two vectors.

By the use of the 1-Hz measurement frequency as the nominal case, the footprint of the reference trajectory was analyzed over a range of terminal observed altitudes (TOA). Figure 7 shows the footprints for the 1-Hz case at TOA values of 50, 70, and 90 km. Figures 7 clearly show that the footprint is along the ground track and gets exponentially larger with increasing TOA. Table 4 summarizes the footprint statistics for the nominal (1-Hz) case and Table 5 summarizes the footprint statistics for the range of measurement frequencies and a TOA of 50 km. In summary, Tables 4 and 5 show that the accuracy of the prediction scheme improves dramatically at lower TOAs and higher measurement frequencies. In all cases, however, the reference point of impact is within the footprint. Therefore, it can be stated with 99% certainty that, for a given scenario, the true location of impact will be within the $3\sigma$ bounds of the associated footprint and that the optimal estimate is a reliable prediction of the location of impact.

**Table 4 Footprint statistics for nominal entry (measurement frequency = 1 Hz)**

| TOA, km | Optimal impact estimation error, km | $3\sigma$ Longitude, ° | $3\sigma$ Latitude, ° | Approximate area, km$^2$ |
|---|---|---|---|---|
| 50 | 5.07 | 0.50 | 0.15 | 90 |
| 60 | 5.79 | 0.56 | 0.17 | 60 |
| 70 | 69.43 | 1.04 | 0.31 | 150 |
| 80 | 38.38 | 2.31 | 0.68 | 250 |
| 90 | 42.55 | 5.35 | 1.53 | 600 |
| 100 | 1372.91 | 21.99 | 11.14 | 7500 |

**Table 5 Footprint statistics for various measurement frequencies (TOA = 50 km)**

| Frequency, Hz | Optimal impact estimation error, km | $3\sigma$ Longitude, ° | $3\sigma$ Latitude, ° | Approximate area, km$^2$ |
|---|---|---|---|---|
| 0.2 | 14.64 | 0.46 | 0.14 | 100 |
| 0.5 | 7.70 | 0.27 | 0.08 | 60 |
| 1 | 5.07 | 0.50 | 0.15 | 90 |
| 2 | 4.97 | 0.59 | 0.18 | 150 |

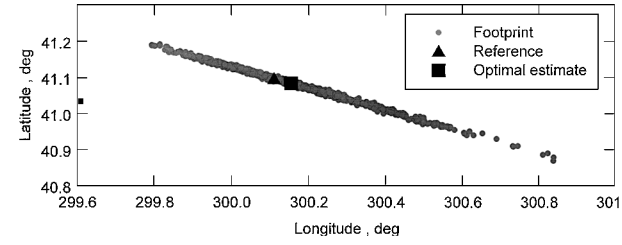


**TOA = 50 km**

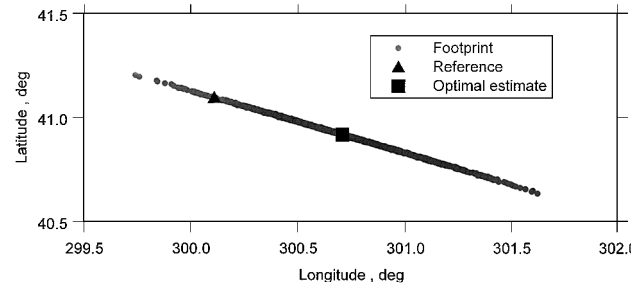


**TOA = 70 km**

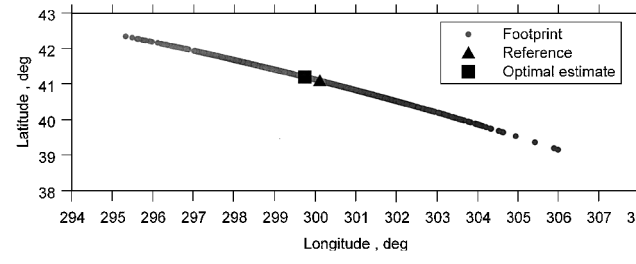


**TOA = 90 km**

**Fig. 7 Impact footprint for nominal reentry trajectory.**

## Summary

A ground-based method for estimating and predicting the reentry trajectories of orbital debris has been presented. Estimation is accomplished through the use of an extended Kalman filter and RTS smoother. Lift and drag ballistic coefficients are appended to the state vector and the corresponding augmented state is modeled with dynamic integral noise. Subsequently, a Monte Carlo simulation is

used to predict the location of impact, with the final error covariance matrix from the estimation stage as the basis for computing the dispersed initial conditions.

Results are heavily dependent on tracking gaps, multiple station coverage, and measurement frequency, but for those cases with a sufficient amount of coverage, the time-varying ballistic coefficients can be determined to within a few percent of their true values. In addition, a Monte Carlo simulation demonstrated that, under these circumstances, the impact footprint can be accurately predicted, with the best prediction of impact within kilometers of the true value. This prediction scheme appears to be accurate under most circumstances, although its effectiveness is dependent on measurement frequency and terminal observed altitude.

Future work should focus on modifying the filter dynamics to account for lateral wind forces and other perturbations. In addition, it may prove beneficial to utilize alternate filtering schemes (such as a square-root information filter) and a systematic investigation of filter tuning.

## Acknowledgments

The authors would like to thank Anil V. Rao for discussions involving the estimation scheme and Christopher K. Wikle for his guidance in implementing the Monte Carlo impact prediction scheme.

## References

[1]Wang, L. Q., and Stark, J. P. W., "Direct Simulation of Space Debris Evolution," *Journal of Spacecraft and Rockets*, Vol. 36, No. 1, 1999, pp. 114–123.

[2]Sridharan, R., Beavers, W., Gaposchkin, E. M., Lambour, R., Kansky, J., and Stansbery, E., "Radar and Optical Characterization of an Anomalous Orbital Debris Population," *Journal of Spacecraft and Rockets*, Vol. 36, No. 5, 1999, pp. 719–725.

[3]Pardini, C., and Anselmo, L., "Assessing the Risk of Orbital Debris Impact," *Space Debris*, Vol. 1, No. 1, 1999, pp. 37–43.

[4]Pardini, C., Anselmo, L., Rossi, A., Cordelli, A., and Farinella, P., "New Orbital Debris Reference Model," *Journal of the Astronautical Sciences*, Vol. 46, No. 3, 1998, pp. 249–265.

[5]Sato, T., "Shape Estimation of Space Debris Using Single-Range Doppler Interferometry," *IEEE Transactions on Geoscience and Remote Sensing*, Vol. 37, No. 2, 1999, pp. 1000–1005.

[6]Swinerd, G. G., Barrows, S. P., and Crowther, R., "Short-Term Debris Risk to Large Satellite Constellations," *Journal of Guidance, Control, and Dynamics*, Vol. 22, No. 2, 1999, pp. 291–295.

[7]Mehra, R. K., "A Comparison of Several Nonlinear Filters for Reentry Vehicle Tracking," *IEEE Transactions on Automatic Control*, Vol. 16, No. 4, 1971, pp. 307–319.

[8]Trujillo, B. M., "Determination of Lift and Drag Characteristics of Space Shuttle Orbiter Using Maximum Likelihood Estimation Technique," AIAA Paper 86-2225, Aug. 1986.

[9]Cardillo, G. P., Mrstik, A. V., and Plambeck, T., "A Track Filter for Reentry Objects with Uncertain Drag," *IEEE Transactions on Aerospace and Electronic Systems*, Vol. 35, No. 2, 1999, pp. 394–409.

[10]Rao, A. V., "Minimum-Variance Estimation of Reentry Debris Trajectories," *Journal of Spacecraft and Rockets*, Vol. 37, No. 3, 2000, pp. 366–373.

[11]Lee, D.-J., and Alfriend, K. T., "Effects of Atmospheric Density Uncertainty on the Probability of Collision," AIAA Paper 2000-181, Jan. 2000.

[12]Gelb, A. (ed.), *Applied Optimal Estimation*, 1st ed., MIT Press, Cambridge, MA, 1974, pp. 182–188.

[13]Brown, R. G., *Introduction to Random Signal Analysis and Kalman Filtering*, 1st ed., Wiley, New York, 1983, pp. 275–280.

[14]Vallado, D. A., *Fundamentals of Astrodynamics and Applications*, 1st ed., McGraw–Hill, New York, 1997, pp. 651–658.

[15]Majors, J. M., "Upgrading the Nation's Largest Space Surveillance Radar," URL: http://www.swri.org/3pubs/brochure/d10/survrad/survrad.htm [cited 24 April 2002].

D. B. Spencer
*Associate Editor*